Neuro-Oncology
25(1), 82–96, 2023 | https://doi.org/10.1093/neuonc/noac157 | Advance Access date 21 June 2022

Oct4A palmitoylation modulates tumorigenicity and stemness in human glioblastoma cells

Xueran Chen, Wanxiang Niu, Xiaoqing Fan, Haoran Yang, Chenggang Zhao, Junqi Fan, Xuebiao Yao, and Zhiyou Fang

Anhui Province Key Laboratory of Medical Physics and Technology; Institute of Health and Medical Technology, Hefei Institutes of Physical Science, Chinese Academy of Sciences, Hefei, China (X.C., W.N., X.F., H.Y., C.Z., J.F., Z.F); Science Island Branch, Graduate School of University of Science and Technology of China, Hefei, China (X.C., W.N., X.F, C.Z., J.F.); Department of Laboratory Medicine, Hefei Cancer Hospital, Chinese Academy of Sciences, Hefei, China (X.C., H.Y., Z.F); Department of Anesthesiology, The First Affiliated Hospital of USTC, Division of Life Sciences and Medicine, University of Science and Technology of China (USTC), Hefei, China (X.F.); MOE Key Laboratory for Cellular Dynamics, University of Science & Technology of China, Hefei, China (X.Y.)

Corresponding Authors: Xueran Chen, PhD, Anhui Province Key Laboratory of Medical Physics and Technology; Institute of Health and Medical Technology, Hefei Institutes of Physical Science, Chinese Academy of Sciences, No. 350, Shushan Hu Road, Hefei, Anhui 230031, China (xueranchen@cmpt.ac.cn); Xuebiao Yao, PhD, MOE Key Laboratory for Cellular Dynamics, University of Science & Technology of China, No.96, Jin Zhai Road, Hefei, Anhui 230027, China (yaoxb@ustc.edu.cn); Zhiyou Fang, PhD, Anhui Province Key Laboratory of Medical Physics and Technology; Institute of Health and Medical Technology, Hefei Institutes of Physical Science, Chinese Academy of Sciences, No. 350, Shushan Hu Road, Hefei, Anhui 230031, China (z.fang@cmpt.ac.cn).

Abstract

Background. Glioblastoma multiforme and other solid malignancies are heterogeneous, containing subpopulations of tumor cells that exhibit stem characteristics. Oct4, also known as POU5F1, is a key transcription factor in the self-renewal, proliferation, and differentiation of stem cells. Although it has been detected in advanced gliomas, the biological function of Oct4, and transcriptional machinery maintained by the stemness of Oct4 protein-mediated glioma stem cells (GSC), has not been fully determined.

Methods. The expression of Oct4 variants was evaluated in brain cancer cell lines, and in brain tumor tissues, by quantitative real-time PCR, western blotting, and immunohistochemical analysis. The palmitoylation level of Oct4A was determined by the acyl-biotin exchange method, and the effects of palmitoylation Oct4A on GSCs were investigated by a series of in vitro (neuro-sphere formation assay, double immunofluorescence, pharmacological treatment, luciferase assay, and coimmunoprecipitation) and in vivo (xenograft model) experiments.

Results. Here, we report that all three variants of Oct4 are expressed in different types of cerebral cancer, while Oct4A is important for maintaining tumorigenicity in GSCs. Palmitoylation mediated by ZDHHC17 was indispensable for preserving Oct4A from lysosome degradation to maintain its protein stability. Oct4A palmitoylation also helped to integrate Sox4 and Oct4A in the SOX2 enhancement subregion to maintain the stem performance of GSCs. We also designed Oct4A palmitoylation competitive inhibitors, inhibiting the self-renewal ability and tumorigenicity of GSCs.

Conclusions. These findings indicate that Oct4A acts on the tumorigenic activity of glioblastoma, and Oct4A palmitoylation is a candidate therapeutic target.

Key Points

- Palmitoylation mediated by ZDHHC17 could protect Oct4A from lysosomal degradation, and thereby maintaining its protein stability.
- Oct4A palmitoylation contributed to the integration of Sox4 and Oct4A at the SOX2 enhancer region.

Importance of the Study

Although Oct4 has been detected in high-grade gliomas, the transcriptional mechanism to maintain glioma stem cells (GSCs), mediated by Oct4 protein, remains to be fully determined. Protein palmitoylation mediated by ZDHHC17 is essential to prevent Oct4A lysosomal degradation to maintain its protein stability and is conducive to the formation of complexes between SOX4 and Oct4A. We also designed a competitive Oct4A palmitoylation inhibitor to inhibit the self-renewal ability and tumorigenicity of GSC. Therefore, our findings suggest that Oct4A plays a role in the tumorigenic activity of glioblastoma, and Oct4A palmitoylation may be a candidate therapeutic target.

Glioblastoma multiforme (GBM) is the most invasive form of malignant glioma and is one of the most malignant human cancers, with an estimated median survival time of approximately 1 year.[1,2] Like other types of tumor cells, glioma stem cells (GSCs) have been isolated from human glioblastoma and have been found to have strong resistance to chemotherapy and radiotherapy.[3,4] The failure to cure glioblastoma may be due to existing treatment strategies only affecting the tumor volume rather than the GSCs. These findings indicate that an innovative treatment strategy is required to achieve functional eradication of GSCs.

Oct4, also known as POU5F1, is a transcription factor involved in the pluripotency of stem cells.[5,6] The gene encodes three isoforms—Oct4A, Oct4B, and Oct4B1—through alternative splicing. Oct4A can be translated into a protein (360 amino acids), while Oct4B and Oct4B1 can generate up to three proteins (265, 190, and 164 amino acids, respectively) by using different translation initiation sites.[7,8] Although Oct4 has been detected in high-grade glioma, the exact expression pattern and biological function of its isoform are still largely unknown[9,10]; moreover, the transcriptional machinery for maintaining the stemness of GSCs—mediated by the Oct4 protein—is also yet to be fully determined.

Protein S-palmitoylation refers to a two-sided, posttranslational modification of proteins and fatty acids; it is regulated by protein acyltransferase and characterized by a conserved, Asp-His-His-Cys (DHHC) catalytic domain.[11,12] Many recent studies have shown that DHHC protein and its substrate play a key role in tumorigenesis,[13,14] especially in the development and malignant progression of glioma.[15,16] Here, we report that all three variants of Oct4 are expressed in different types of brain cancer, and Oct4A is the key factor in maintaining the tumorigenic activity of GSCs. Palmitoylation—mediated by ZDHHC17—was found to be indispensable, protecting Oct4A from lysosomal degradation and thereby maintaining its protein stability. Oct4A palmitoylation also contributed to the integration of Sox4 and Oct4A at the SOX2 enhancer region, thereby maintaining the stemness properties of GSCs. We also designed a competitive inhibitor for Oct4A palmitoylation that suppresses the self-renewal capacity and tumorigenicity of GSCs. Our findings thus indicate that Oct4A plays a role in the tumorigenic activity of glioblastoma, while Oct4A palmitoylation may be a candidate therapeutic target.

Materials and Methods

Ethics Statement

Tumor tissues were obtained from Hefei Cancer Hospital, Chinese Academy of Sciences, and tumor characteristics and clinical information are presented in Supplementary Table 1. The study was approved by the institutional review board of Hefei Cancer Hospital, Chinese Academy of Sciences (approval number, SWYX-Y-2021-41). All animal experiments were performed according to the guidelines of the Animal Use and Care Committees at the Hefei Institutes of Physical Science, Chinese Academy of Sciences (approval number, SWYX-DW-2021-37).

Reagents, Antibodies, and Plasmids

The palmitate analog inhibitor, 2-bromopalmitate (2-BP, 238422), and general depalmitoylation inhibitor, palmostatin B (PalmB, 178501), were purchased from Sigma-Aldrich (St. Louis, MO, USA). The DNA methylation inhibitor, 5-aza-2′-deoxycytidine (5′-Aza, HY-A0004); lysosomal inhibitors, leupeptin (HY-18234A) and bafilomycin A1 (HY-100558); and a proteasome inhibitor, MG132 (HY-13259), were purchased from MedChemExpress (Middlesex County, NJ, USA).

Two Oct4 antibodies were used: a mouse monoclonal antibody that recognizes amino acids 1-134 of human Oct4 (sc-5279; Santa Cruz Biotechnology, Inc., Dallas, TX, USA), and a rabbit polyclonal antibody that recognizes the C-terminus of Oct4 (ab19857; Abcam, Cambridge, UK). Anti-Sox2 (3579), anti-Sox17 (81778), anti-MAP2a/b/c (8707), anti-glial fibrillary acidic protein (anti-GFAP) (3670), and anti-β-actin (3700) antibodies were purchased from Cell Signaling Technology, Inc. (Danvers, MA, USA). Anti-ZDHHC17 (SAB2500508), anti-Sox4 (SAB2108306), anti-GFP (G6539), and anti-HA (H9658) antibodies were obtained from Sigma-Aldrich.

For overexpression studies, full-length Oct4A or Oct4B-265 cDNA were cloned into pEGFP-C3 expression vectors (Invitrogen, Waltham, MA, USA), while HA-tagged Oct4A cDNA was cloned into pCDNA3.0 expression vectors (Invitrogen), and all constructs were verified via DNA sequencing. Subsequently, the vector constructs were transfected into the cells using Lipofectamine 2000 Transfection Reagent (Invitrogen) based on the manufacturer's instructions.

Recombinant lentiviral particles were generated using the plasmids pLKO.1, pMD2.G, and psPAX2 provided by Addgene and maintained in *E. coli* Stbl3 (Invitrogen, Carlsbad, CA). The anti-Oct4A RNAi was 5′-UCACCUU CCCUCCAACCAGUUGCCC-3′ and the anti-Oct4B RNAi was 5′-AAGGGAUGCAGAGCAUCGUGAAAGG-3′. The cells were treated with puromycin (0.5 μg/mL; #A1113802, Thermo Fisher Scientific) for the establishment of stable cell lines over 1 week.

T98G cells with Oct4A Cys198 mutation to Ala were generated using the Invitrogen CRISPR reagents and primarily included a guide RNA (gRNA) (5′-TCAAGAACATGTGTAAG CTG-3′), a donor DNA (5′-GCTTTGAGGCTCTGCAGCTTA GCTTCAAGAACATGGCTAAGCTGCGGCCCTTGCTGCAG AAGTGGGTGGAGGAAGC-3′) and a TrueCut Cas9 Protein (also called Cas9 Nuclease). All reagents were delivered to cells with Lipofectamine CRISPRMAX Cas9 Transfection Reagent, based on the manufacturer's instructions. To evaluate the gene editing activity of gRNA, the genomic DNA of gRNA-transfected cells was extracted, and the Oct4A gene was amplified using sequence-specific primers: forward, 5′-CTGCAGATTCTGACCGCATC-3′, and reverse, 5′-CCATCCCACTGAGAACCACT-3′. The cells were cultured in a medium containing 0.5 μg/mL puromycin, selected, passaged, and confirmed via DNA sequencing.

Cell Culture

All glioma cells (U87MG, T98G, LN18, A712, SF126, and U118MG) used in this study were obtained from Cellcook (Guangzhou, China) and were cultured in Dulbecco's modified Eagle medium (Gibco, USA) containing 10% fetal bovine serum (HyClone, USA). The U87 GSCs, T98G GSCs, and A172 GSCs were derived from U87, T98G, and A172 cells, respectively, and the biological characteristics were analyzed, as shown in Supplementary Figure 1. These GSCs had high stemness marker expression, sphere formation ability, and tumor-initiating potential. GBM0378 and GBM1492 GSCs were isolated from surgical specimens in an earlier study and confirmed.[16] GBM0378, GBM1492, and T98G GSCs were cultured in neurobasal medium (without retinoic acid) containing B27 (Invitrogen), basic fibroblast growth factor (10 ng/mL), and epidermal growth factor (10 ng/mL). All cell lines used in this study were analyzed by short tandem repeat typing and mycoplasma serology (most recently in February 2021), passaged 2-6 times for experimental use, and revived every 3-4 months.

Glioma Tissue Microarray and Immunohistochemistry Staining

Glioma tissue microarrays were obtained from US Biomax, Inc. (Rockville, MD, USA), containing 210 glioma and 15 normal samples. Tumor samples were pathologically graded as low-grade tumors (42) and GBM (168) on the basis of WHO's criteria. Tumor characteristics and clinical information are presented in Supplementary Table 2. Immunohistochemical analyses of glioma tissue microarrays were performed as described previously.[15,16] KF-PRO Digital Slide Scanning System (Kongfong Biotech International Co., Ltd., Ningbo, China) was used to visualize signals. The results of immunohistochemistry (IHC) staining were evaluated by two independent pathologists with no prior knowledge of patients' characteristics. Discrepancies were resolved by consensus. The staining extent score was on a scale of 0-4, corresponding to the immunoreactive percentage of tumor cells (0%, 1%-5%, 6%-25%, 26%-5%, and 76%-100%, respectively). The staining intensity was represented as negative (score = 1), weak (score = 2), or strong (score = 3). A score that ranged from 0 to 12 was calculated by multiplying the staining extent score with the intensity score, leading to a low (0-4) or a high (8-12) level value for each specimen.

Real-time Reverse Transcriptase-Polymerase Chain Reaction (qRT-PCR)

Total RNA was isolated using an RNAqueous-Midi Total RNA Isolation Kit (AM1911, Invitrogen), and a real-time polymerase chain reaction was performed on a 7300 Cycler (Applied Biosystems, Waltham, MA, USA) using the VetMAX-Plus One-Step RT-PCR Kit (4415328, Applied Biosystems). Each sample was thrice replicated, and the expression of the target gene was calculated by the $2^{-\Delta\Delta Ct}$ method. β-actin was used as the internal control. The gene-specific primer sequences used in the study are listed in Supplementary Table 3.

Immunoprecipitation, Acyl-biotin Exchange Labeling, and Western Blot Analysis

Protein-protein interactions were detected using a Dynabeads Co-Immunoprecipitation Kit (Invitrogen). The immunoprecipitated and coimmunoprecipitated proteins were analyzed by SDS-PAGE and western blotting, respectively.

To determine the level of protein palmitoylation, acyl-biotin exchange (ABE) assays were performed as previously described.[15,16] In brief, immunoprecipitated beads were incubated with washing buffer supplemented with 50 mM *N*-ethylmaleimide (50 mM Tris, pH 7.4, including 5 mM EDTA, 150 mM NaCl, and 1% Triton X-100) at 4°C for 1 hour. Next, the beads were incubated with 1 M hydroxylamine (pH 7.4) at room temperature for 1 hour, and then exposed to 0.5 μM 1-biotinamido-4-(4′-[maleimidomethylcyclohexane]-formamide) butane (pH 6.2) for 1 hour at 4°C. Samples were analyzed by SDS-PAGE and western blotting.

Cell lysate was quantified by dicinonic-acid assay, analyzed by SDS-PAGE, and transferred to a nitrocellulose-imprinted membrane (Pall Corporation, New York, NY, USA), followed by incubation with primary antibody. The membrane was then exposed to the corresponding horseradish-peroxidase-coupled secondary antibody (Invitrogen), and the band was detected using enhanced chemiluminescence (Invitrogen).

In Vitro Tumorsphere Formation

For suspension culture/tumorsphere formation, 50, 100, 250, 500, 750, and 1000 cells were seeded in 96-well plates

containing 200 μL of complete neurobasal medium. After 10 days, the tumorspheres were measured and analyzed.

DNA Preparation and Bisulfite Genomic Sequencing

Genomic DNA was extracted from frozen tissues using the PureLink Genomic DNA Mini Kit (Invitrogen), and the extracted DNA was treated with sodium bisulfite as previously described.[17] The primers (forward: 5′-GGATTTGTATTGAGG TTTTGGAG-3′, reverse: 5′-TAACCCATCACCTCCACCAC-3′) were designed to amplify the Oct4 promoter and exon 1 from −234 to +46 for bisulfite genomic sequencing. The amplified products were purified using the PureLinkPro 96 Genomic DNA Purification Kit (Invitrogen), subjected to TA-cloning using the pEASY-T3 vector (TransGen Biotech Co., Ltd., Beijing, China), and sequenced.

Chromatin Immunoprecipitation-PCR

Chromatin immunoprecipitation (ChIP) was performed as described previously.[18] Briefly, sheared chromatin (sonicated to 200-500 bp) from about 5 × 10^6 cells was fixed in 1% formaldehyde and incubated with 2 μg of the antibody overnight at 4°C. Following reverse crosslinking, DNA was treated with proteinase K and purified using a PCR Purification Kit (QIAGEN), eluted, and used for qPCR. The SOX2 enhancer region was +3553 through +4290. PCR primers for Sox2 (+4089~+4289) was as follows: forward, 5′-GGATAACATTGTACTGGGAAGGGACA-3′, reverse 5′-CAAAGTTTCTTTTATTCGTATGTGTGAGCA-3′.

Animal Experiments

Six-week-old female BALB/c immunodeficient nude mice weighing approximately 18-25 g were anesthetized by intraperitoneal injection of ketamine (132 mg/kg) and methylthiazide (8.8 mg/kg). The T98G glioma cells (1000 cells, 0.1 mL), or T98G GSCs (100-5000 cells, 0.1 mL) suspensions were subcutaneously injected in the upper right flanks. For the Oct4A palmitoylation blockade group, cell suspensions were treated with CPP-S1, a competitive peptide inhibitor (QLSFKNMCKLRPLLQ) for 6 hours before injection. The peptide containing the C198A mutation was considered the control. Tumors were measured every 5 days, starting on day 5. Tumor volume was calculated using the formula: 1/2 × D × d2 (D and d represent the major and minor axes, respectively). At the last indicated time point, the tumor-bearing mice were sacrificed, and the tumor weights were measured.

T98G GSCs were transduced with lentivirus containing luciferase and were treated with CPP-S0 or CPP-S1 for 6 hours before intracranial implantation. Subsequently, the suspension of 1000 cells (2 μL) in phosphate-buffered saline containing high glucose was stereotactically injected into the hemistriatum of BALB/c immunodeficient nude mice at 6 weeks of age. The co-ordinate parameters adopted were as follows: dorsoventral = −3.5 mm; mediolateral = +2.5 mm; anteroposterior = 0. Luciferin was injected into the peritoneal cavity to track tumor cells in vivo in the post-injection period of around 5 weeks. Animals were anesthetized using sodium pentobarbital (50 mg/kg) and the IVIS Lumina System was used for bioluminescence imaging (PerkinElmer).

Statistical Analysis

All data were analyzed using GraphPad Prism software. Data were shown as means ± standard deviation. The levels of significance for comparison between samples were determined by Student's *t* test. The significance of the growth curve of xenografts between the groups was analyzed by one-way analysis of variance. The $P > .05$ value was considered not significant (ns). $^*P < .05$, $^*P < .01$, $^{***}P < .001$.

Results

Expression of Oct4 Variants in Human Glioma

The human *Oct4* gene encodes three isoforms, generated by alternative splicing: Oct4A, Oct4B, and Oct4B1 (Figure 1A). The Oct4A transcript comprises exons 1, 2b, 2d, 3, and 4; exon 1 represents a unique portion of Oct4A. Compared with Oct4A, Oct4B has exon 2a, while the Oct4B1 transcript is similar to Oct4Ba and contains additional exon 2c. The *Oct4A* gene encodes a unique protein consisting of 360 amino acids, while the *Oct4B* and *Oct4B1* genes can produce three proteins—consisting of 265, 190, or 164 amino acids—through the use of different transitional start sites.

First, we examined the expression of Oct4 spliced variants in brain cancer tissues. Our results showed that all three isoforms were expressed in different types of brain cancer tissues. In addition, compared with other types of brain tumors, their expression in glioma tissues was significantly higher (Figure 1B). In contrast, in the Oct4B1 variant, both Oct4A and Oct4B expressions were significantly higher in high-grade gliomas (grade III-IV) than that in low-grade gliomas (grade I-II) (Figure 1C). Notably, the expression of Oct4A in specimens with recurrent glioma was significantly higher than that in specimens with newly diagnosed glioma.

Next, we examined the expression of Oct4 variants in human GSCs and glioblastoma cell lines (Figure 1D). Oct4B expression in most glioblastoma cells was higher than that in the GSCs, and Oct4B1 mRNA was abundantly expressed. While Oct4A mRNA was expressed in both, its level was slightly higher in GSCs than in glioblastoma cells. Analysis using the TCGA Research Network revealed that Oct4 mutations rarely occurred in lower-grade gliomas or GBM (Figure 1E). Indeed, the Oct4 promoter region contained 11 cytosine-phosphate-guanine dinucleotides (Figure 1F). DNA methylation levels in recurrent glioma (56.43% ± 12.16%) decreased noticeably compared with that in newly diagnosed (64.72% ± 11.17%) and low-grade (72.27% ± 10.24%) glioma (Figure 1G). Following 5′-Aza treatment, Oct4 mRNA expression in both U87MG and LN18 cells was highly upregulated, compared with cells without Aza treatment (Figure 1H). Consistent with this, 5′-Aza treatment significantly increased Oct4A protein expression, although it slightly decreased 32-hour post-treatment (Supplementary

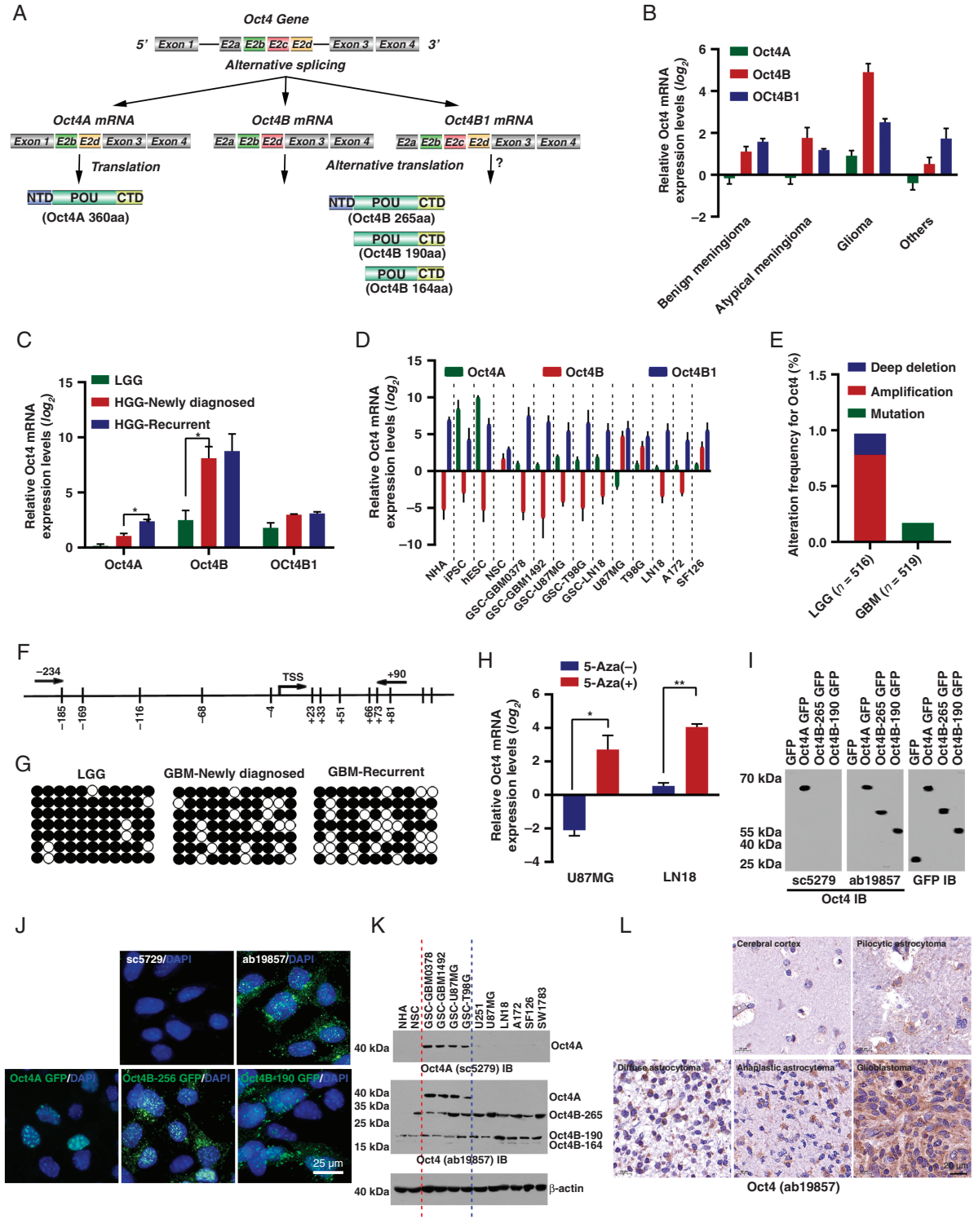

Fig. 1 Structure of Oct4 variants and their expression pattern in human brain tumors, glioblastoma stem cells, and glioblastoma cells. (A) A schematic diagram showing transcripted mRNAs and proteins expressed by the human *Oct4* gene. (B) Histograms of the relative expression of Oct4 variants in different types of brain tumors were obtained via quantitative real-time polymerase chain reaction (qRT-PCR). Benign meningioma (grade I, n = 10). Atypical meningioma (grade II, n = 8). Grade III-IV glioma (n = 21). Others, craniopharyngioma (n = 4), schwannoma (n = 5), and anaplastic meningioma (n = 4). (C) Histograms of the relative expression of Oct4-spliced variants in low-grade glioma (grade I-III, n = 23), newly diagnosed high-grade glioma (HGG) (grade III-IV, n = 9), and recurrent HGG (n = 7) were obtained via qRT-PCR. (D) Histograms of the relative expression of Oct4 variants in induced pluripotent cells, embryonic stem cells (iPSCs), neural stem cells (NSCs), normal human astrocytes (NHA), glioblastoma stem cells (GSCs) (GSC-GBM0378, GSC-GM1492, GSC-U87MG, GSC-T98G, GSC-LN18), and glioblastoma cells (U87MG, T98G, LN18, A172, SF126) were obtained via qRT-PCR. (E) The graphs represent Oct4

Figure 2A and B). Along with the Oct4A mRNA expression increase in GSCs, the methylation level of Oct4 promoter region was reduced during the GSCs' self-renewal stage. At differentiation stage, Oct4A mRNA expression was reduced, and its methylation was increased (Supplementary Figure 2C and D). DNMT3A may be an important regulator for methylation of the Oct4 promoter region because only DNMT3A knockdown could enhance the expression of Oct4, whereas other DNMT family members could not (Supplementary Figure 2E). These results suggest that DNA hypomethylation may be a key mechanism underlying Oct4 upregulation in high-grade gliomas and glioma recurrence.

Localization of Oct4 Isoforms in Human Glioblastoma Cells and Tissues

To examine the biological function of Oct4 isoforms, we constructed GFP-tagged Oct4A, Oct4B-265, and Oct4B-190 constructs, and overexpressed them in LN18 glioblastoma cells. The mouse monoclonal antibody, sc-5279, could only recognize Oct4A, while the rabbit polyclonal antibody, ab19857, could recognize both Oct4A and Oct4B (Figure 1I). Analysis via immunofluorescence revealed that Oct4A was localized in the nucleus, whereas Oct4B was localized in both the cytoplasm and nucleus (Figure 1J). Analysis via western blotting revealed that Oct4A was only expressed in GSCs, while Oct4B was expressed in neural stem cells (NSCs), GSCs, and more differentiated glioblastoma cells; additionally, expressions of Oct4B-265 and Oct4B-190 were higher in the glioblastoma cells than those in the NSCs and GSCs (Figure 1K). Antibody sc-5279 rarely recognized Oct4 signals in glioma tissues, whereas the ab19857 antibody results revealed that expression of Oct4 was progressively elevated in and highly correlated with glioma samples of grades I-IV, compared with normal brain tissue (Figure 1L).

Oct4A Palmitoylation in Human Glioblastoma Stem Cells

Oct4A mRNA was expressed in both the GSCs and more differentiated glioblastoma cells, whereas the Oct4A protein was only expressed in GSCs; thus, posttranslational modification of Oct4A may occur. Using an online software program (CSS-Palm: csspalm.biocuckoo.org), we revealed a potential palmitoylation site (Cys198, Figure 2A)—highly conserved among different species—as well as other Oct4 isoforms. The acyl-biotinyl exchange (ABE) assay results revealed that Oct4A could be palmitoylated and that the mutation of Cys198 to Ala substantially abolished Oct4A palmitoylation (Figure 2B). Coimmunoprecipitation revealed that Oct4A was associated with ZDHHC3/5/6/17/20 (Figure 2C). Following the depletion of ZDHHC17, the Oct4A palmitoylation level was noticeably downregulated when compared with the knockdown of other ZDHHCs (Figure 2D, Supplementary Figure 3A); ZDHHC17 was therefore considered a potential enzyme to interact with and palmitoylate Oct4A.

Palmitoylation of Oct4A Is Critical to the Stability of Oct4A Protein

We subsequently investigated whether palmitoylation modification was responsible for Oct4A protein activity. The palmitate analog, 2-BP—a general inhibitor of palmitoyl in protein—was used to treat T98G GSCs. We also confirmed that 2-BP treatment significantly inhibited palmitoylation of Oct4A (Figure 2E) and inhibited the expression of Oct4A protein in a dose- and time-dependent manner (Figure 2F). It is worth noting that 2-BP treatment did not affect the level of Oct4A mRNA (Figure 2G). In patient-derived GSCs, the abundance of Oct4A protein also decreased significantly after 2-BP treatment (Figure 2H, Supplementary Figure 3B).

To determine how palmitoylation of protein affects the stability of Oct4A, we monitored the degradation kinetics of the endogenous Oct4A level after 2-BP treatment by using cycloheximide-tracing analysis. The level of Oct4A protein decreased rapidly at the beginning of cycloheximide treatment. Its half-life was reduced to 1.5 hours in 2-BP-treated cells and 6 hours in dimethyl sulfoxide-treated cells (Figure 2I). The rate of Oct4A degradation in 2-BP- and ethanol-treated cells corresponds to 6-12 hours after cycloheximide treatment, which may be due to the gradual decrease of 2-BP inhibition (removal from culture medium before starting cycloheximide tracking). To further confirm these results, the stability of wild-type Oct4A and non-palmitoylated Oct4A Cys198A mutant with an HA tag were analyzed. Compared with HA-Oct4A, HA-Oct4A Cys198A protein degrades rapidly, with half-lives of 3 and 8 hours, respectively (Figure 2J). These data conclusively establish that palmitoylation is very important for the stability of the Oct4A protein.

Fig. 1 Continued

mutations in gliomas (TCGA) using cBioPortal. (F) DNA methylation profile of 11 cytosine-phosphate-guanine (CpG) dinucleotides (−234 to +90) located in the Oct4 promoter region. (G) Analysis of DNA methylation at 11 known differentially methylated CpG sites in the Oct4 −234 to +90 region with DNA from low-grade, high-grade, and recurrent gliomas (n = 7). Black and white circles represent methylated and unmethylated sites, respectively. (H) Histograms of the relative expression of Oct4 mRNA in glioma cell lines (U87MG and LN18) treated with 5′-Aza-dc for 72 hours were obtained via qRT-PCR. (I) Western blot analysis demonstrating Oct4 overexpression in T98G glioblastoma cells after being transduced with three lentiviral vectors containing genes for GFP-tagged Oct4 variants. (J) Immunofluorescent analysis showing subcellular localization of three Oct4 isoforms in T98G glioblastoma cells. Oct4 isoforms were labeled with green fluorescence and the nucleus was counterstained with 2-(4-amidinophenyl)-6-indolecarbamidine dihydrochloride (blue). Scale bar = 25 μm. (K) Detection of Oct4 variants (Oct4A and Oct4B) in NSCs, NHAs, GSCs (GSC-GBM0378, GSC-GM1492, GSC-U87MG, GSC-T98G), and glioblastoma cells (U251, U87MG, LN18, A172, SF126, SW1783) by western blotting. (L) detection of Oct4 variants (Oct4A and Oct4B) in different types of brain tumor tissues by immunohistochemistry.

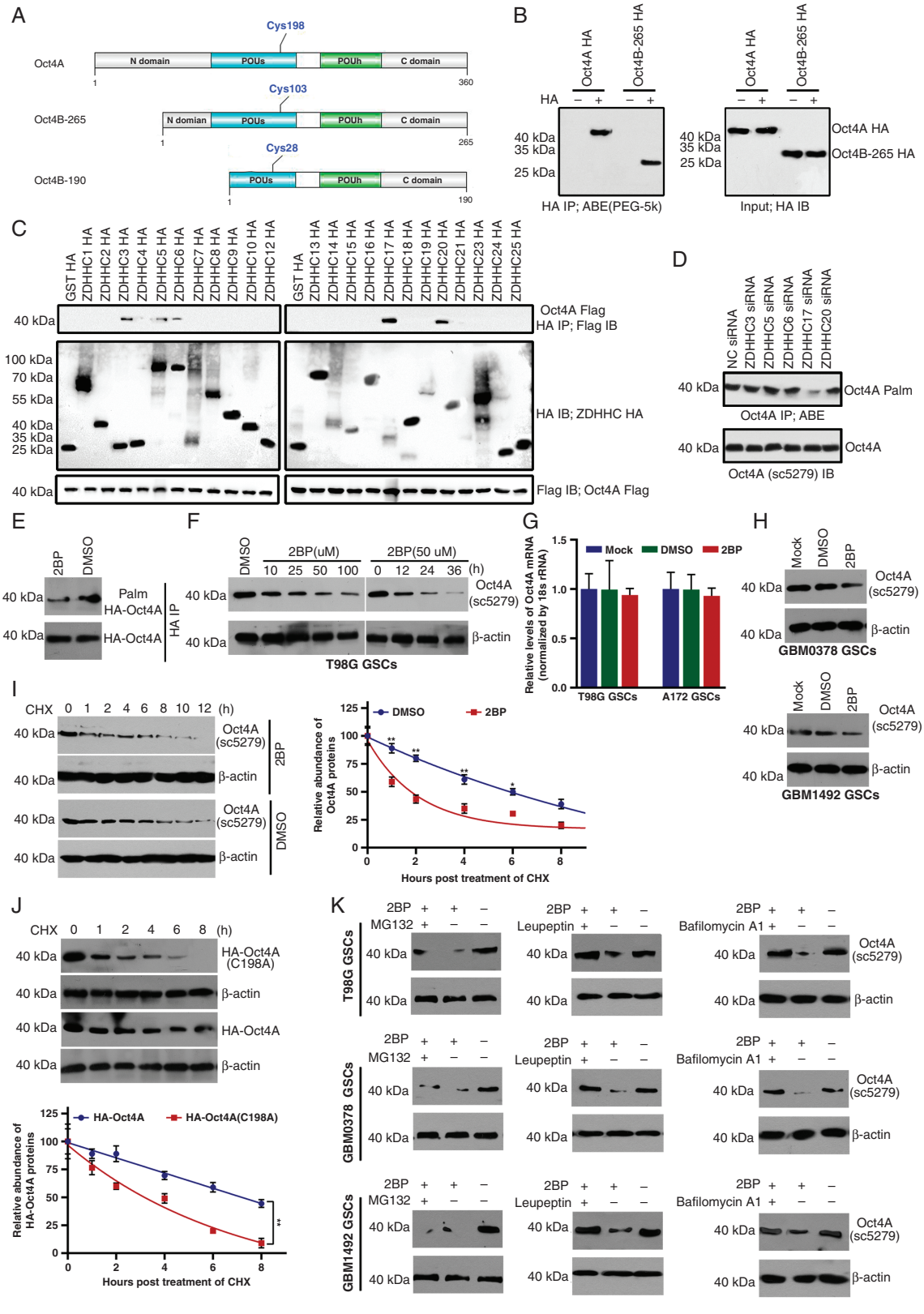

Fig. 2 Association between Oct4A palmitoylation and protein stability. (A) Schematic representation of potential palmitoylation sites of Oct4 variants. (B) Detecting HA-Oct4 palmitoylation using biotin-PEG-5k after performing acyl-biotin exchange (ABE) and immunoprecipitation assays with α-HA beads. (C) Detecting the interaction between Oct4A and 23 HA-tagged ZDHHCs after performing immunoprecipitation assay. HEK293 cells were cotransfected with constructs encoding Flag-Oct4A and HA-ZDHHCs in a 6-well plate. Cell lysates were harvested for immunoprecipitation using

Cell proteins are degraded by ubiquitin-proteasome and/or lysosome pathways for turnover and recovery[19,20]; therefore, we further studied the degradation pathway of Oct4A protein under palmitoyl deficiency. Inhibition of the lysosomal pathway by leupeptin and bafilomycin A1 obviously prevented 2-BP-induced degradation of Oct4A in T98G GSCs (Figure 2K, Supplementary Figure 3C). In contrast, inhibition of the ubiquitin-proteasome pathway by the proteasome inhibitor MG132 failed to prevent Oct4A degradation, indicating that Oct4A was degraded by the lysosome pathway after 2-BP treatment. These results were also confirmed in GSCs from patients (Figure 2K, Supplementary Figure 3C).

Oct4A Palmitoylation Is Essential to Retain Stemness in GSCs

To clarify the role of Oct4A palmitoylation in glioma-initiating cells, we first examined the effect of Oct4A knockdown on their biological characteristics. After Oct4A expression was knocked down with short hairpin RNA (shRNA), T98G GSCs showed a significant decrease in sphere formation ability in a continuous sphere formation test (Figure 3A), and Oct4A overexpression salvaged its decrease (Supplementary Figure 4A). The 2-BP treatment or Oct4A Cys198 mutation to Ala was also confirmed to significantly inhibit the sphere-forming ability of T98G GSCs. However, the capacity for self-renewal was not affected after Oct4B knockdown; thus, these results suggest that Oct4A—especially its palmitoylation—is required for the self-renewal of glioma-initiating cells. In the limiting dilution assay, T98G GSCs with Oct4A shRNA, 2-BP treatment, or Oct4A Cys198A also demonstrated a decreased capacity for self-renewal when compared with the control or Oct4B shRNA-transfected GSCs (Figure 3B). Similar results were obtained using glioma-initiating cells GBM0378 and GBM1492 from other glioblastoma patients (Figure 3B).

According to recent reports, GSCs express neural precursor cell markers, while the expression of neural or glial differentiation markers is rare.[21,22] To examine the expression of these marker proteins in each cell type, spheres in serum-free medium were depolymerized and inoculated onto glass slides coated with poly-L-ornithine and fibronectin. Oct4A knockdown or Oct4A-palmitoylation inhibition downregulated expressions of MEF, ID1, Sox2, and Olig2 (neural precursor cell markers); however, it could upregulate the level of GFAP (an astrocyte differentiated marker) or Tuj1 (a neuronal marker) and MAP2 (a progenitor/neuron marker) (Figure 3C–E, Supplementary Figure 4B). As expected, Oct4A overexpression eliminated the inhibition of stemness marker (Sox2 and Olig2) expression in Oct4A shRNA-GSCs (Supplementary Figure 4C). Results obtained via immunofluorescence also revealed that Oct4A knockdown or Oct4A-palmitoylation inhibition led to a decrease in the number of cells positive for Sox2 and an increase in those for GFAP (Figure 3F); notably, knockdown of Oct4B did not affect their expression. These results indicate that Oct4A palmitoylation was required to maintain the stemness properties of GSCs in vitro.

Palmitoylated Oct4A Interacts With Sox4

Sox2 is known to be a key regulator of the stemness of NSCs and GSCs.[18,23] Results obtained via chromatin immunoprecipitation (ChIP) assays revealed that recruitment of Oct4A to the *SOX2* enhancer element was observed in NSCs and GSCs, although it was weak in NSCs (Figure 4A). In NSC, Sox2 is mainly related to the *SOX2* enhancer element, while Sox4 is mainly combined with the *SOX2* enhancer region. These findings encourage us to explore the interaction between the Sox axis and Oct4A, with regard to the maintenance of GSC stemness properties. Notably, palmitoylated Oct4A interacts synergistically with Sox4 to enhance the activity of the *SOX2* enhancer, whereas the palmitoylated-mutant Oct4A mainly interacted with Sox2 (Figure 4B and C, Supplementary Figure 5A).

Indeed, the excessive Oct4A mRNA levels were not significantly increased by *SOX2* transcriptional activity (Figure 4D). This may have been related to the level of Oct4A palmitoylation, as although ZDHHC17 mRNA level was not associated with Oct4A mRNA level, the ZDHHC17 protein level was positively associated with Oct4A protein level (Figure 4E and F). Notably, the level of Sox2 protein was also positively correlated with that of ZDHHC17 protein (Figure 4G). Consistent with this, ZDHHC17 expression was progressively elevated in grade I-IV glioma specimens compared with that in normal brain tissues (Supplementary Figure 5B and C) and was highly correlated with Oct4A palmitoylation levels in GSCs (Supplementary Figure 5D). Overexpression of ZDHHC17 helps maintain the

Fig. 2 Continued

an anti-HA antibody and then western blot analysis was performed using an anti-Flag antibody. The results of immunoblotting for total Oct4A and HA-ZDHHC proteins are shown. (D) Detecting Oct4A palmitoylation in T98G glioblastoma stem cells (GSCs) treated with ZDHHC3, 5, 6, 17, or 23 siRNA after 48 hours via ABE assays. (E) Detecting palmitoylated HA-Oct4A level in HEK293 cells transfected with HA-Oct4A plasmids for 36 hours, and treated with 30 μM 2-bromopalmitate (2-BP) for 24 hours, via palmitoylation assay. (F) Detecting Oct4A protein expression in T98G GSCs treated with 2-BP at different doses for 24 hours (left panel), or 50 μM for different durations (right panel), by western blotting. (G) Histograms of the relative Oct4 mRNA expression in T98G GSCs and A172 GSCs treated with 50 μM 2-BP for 24 hours were obtained via RT-qPCR. (H) Detecting Oct4A protein expression in GBM0378 GSCs and GBM1492 GSCs treated with 50 μM 2-BP for 24 hours by western blotting. (I) Detecting Oct4A protein expression in T98G GSCs—treated with 50 μM 2-BP or equivalent dimethyl sulfoxide for 24 hours and subsequently subjected to the cycloheximide chase assay—via western blotting (left panel). Relative Oct4A protein levels normalized to β-actin were presented relative to the level (set as 100) at 0-hour post-cycloheximide treatment (right panel). (J) Detecting Oct4A protein expression in T98G GSCs—transfected with plasmids expressing HA-Oct4A or HA-Oct4A C198A for 36 hours and subsequently subjected to cycloheximide chase assay via western blotting. (K) Detecting Oct4A protein expression in T98G GSCs GBM0378 GSCs, and GBM1492 GSCs—treated with 50 μM 2-BP in the presence of 50 μM leupeptin or 100 nM bafilomycin A1 for 24 hours, or 2-BP for 20 hours and subsequently treated with 40 μM MG132 for 4 hours—via western blotting.

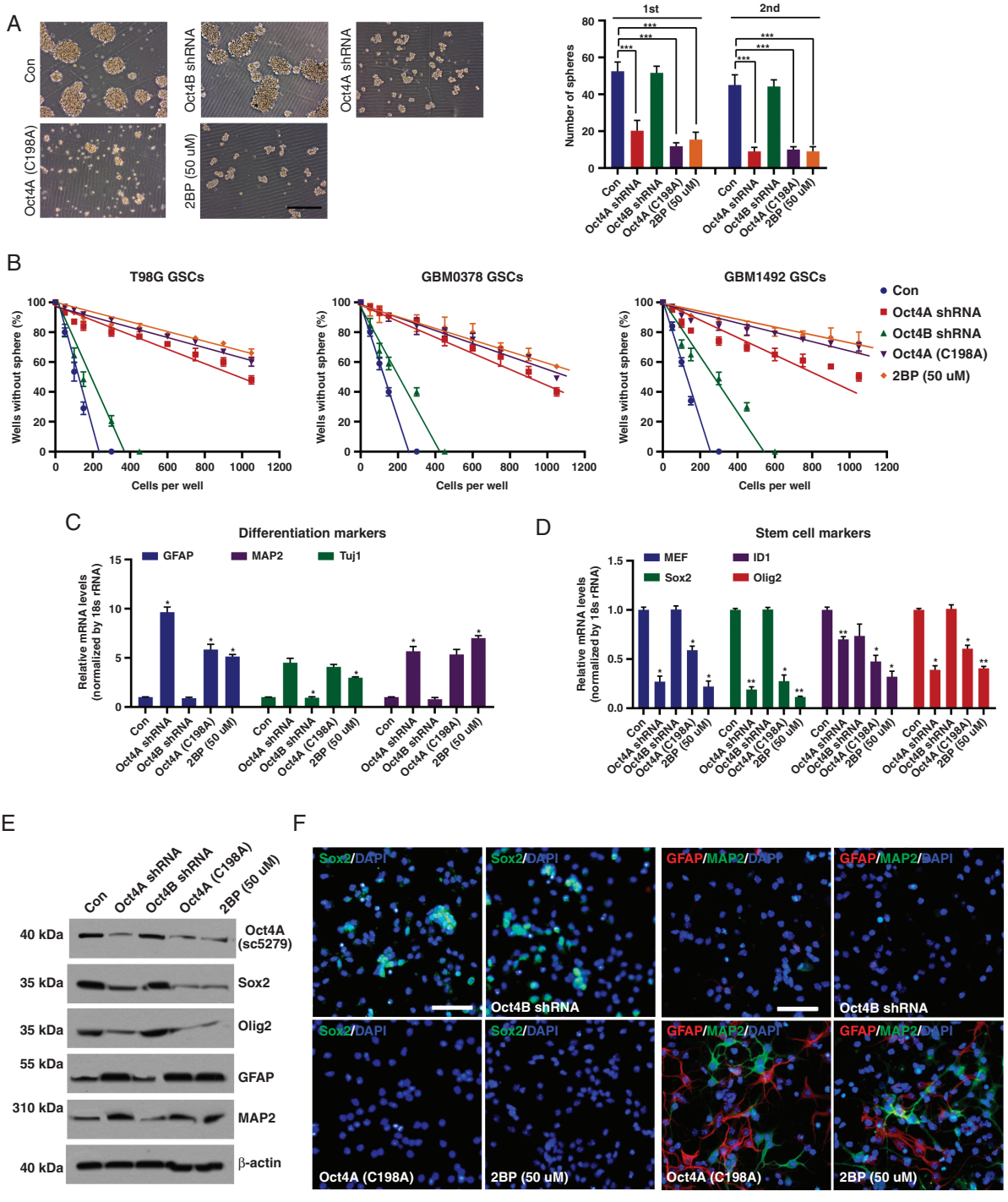

Fig. 3 Oct4A is essential for the retention of stemness of glioma stem cells (GSCs). (A) Detection of glioma spheres formed for T98G GSCs transfected with the control, Oct4A short hairpin RNA (shRNA) duplex, Oct4B shRNA, or Oct4A (C198A), or treated with 50 μM 2-bromopalmitate (2-BP) and cultured for a second passage. Scale bars = 100 μm. (B) Detection of glioma spheres formed for T98G GSCs, GBM0378 GSCs, or GBM1492 GSCs transfected with the control, Oct4A shRNA duplex, Oct4B shRNA, or Oct4A (C198A), or treated with 50 μM 2-BP in the limiting dilution assay. (C) Histograms of the relative MEF, ID1, Sox2, and Olig2 mRNA levels in T98G GSCs, GBM0378 GSCs, or GBM1492 GSCs transfected with the control, Oct4A shRNA duplex, Oct4B shRNA, or Oct4A (C198A), or treated with 50 μM 2-BP were obtained via qRT-PCR. (D) Histograms of the relative MAP2, Tuj1, and GFAP mRNA levels in T98G GSCs, GBM0378 GSCs, or GBM1492 GSCs transfected with the control, Oct4A shRNA duplex, Oct4B shRNA, or Oct4A (C198A), or treated with 50 μM 2-BP were obtained via qRT-PCR. (E) Detection of Oct4A, Sox2, Olig2, GFAP, and MAP2 protein levels in T98G GSCs, GBM0378 GSCs, or GBM1492 GSCs transfected with the control, Oct4A shRNA duplex, Oct4B shRNA, or Oct4A (C198A), or treated with 50 μM 2-BP via western blotting. (F) Immunofluorescent analysis showing subcellular localization of Sox2 at the self-renewal stage, or GFAP and MAP2 at the differentiation stage in T98G GSCs transfected with the control, Oct4A shRNA duplex, Oct4B shRNA, or Oct4A (C198A), or treated with 50 μM 2-BP. Scale bars = 50 μm.

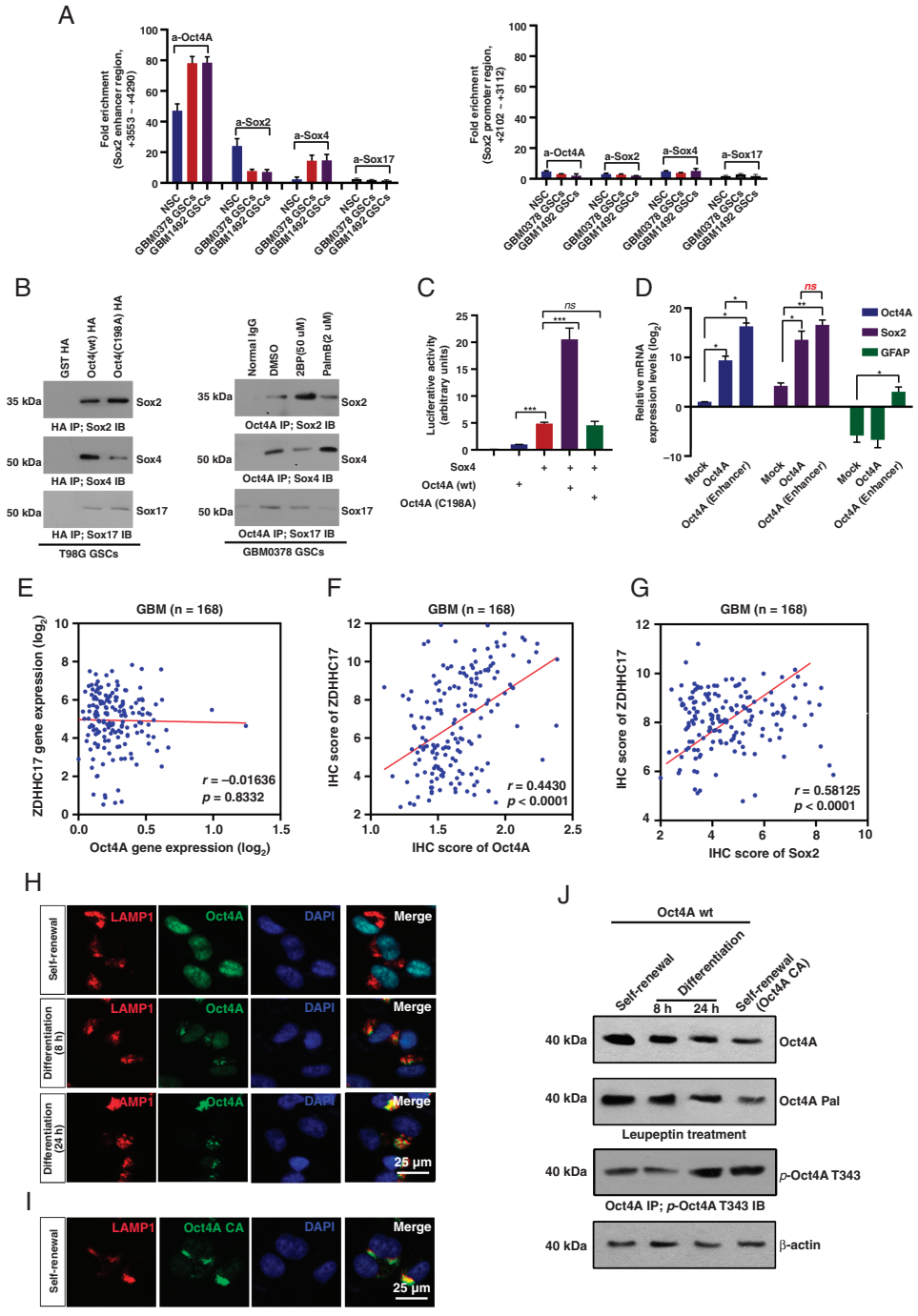

Fig. 4 Oct4A physically interacts with Sox4 at the SOX2 enhancer region. (A) Detecting the recruitment of transcription factors—Oct4A, Sox2, Sox4, or Sox17—to the SOX2 enhancer region (+3553~+4290) using a chromatin immunoprecipitation assay. The SOX2 promoter region (+2102~+3112) was considered as a control. (B) Detecting the interaction between HA-tagged Oct4A (or HA-tagged Oct4A C198A) and Sox-transcriptional factors (Sox2, Sox4, or Sox17) in T98G GSCs (left panel) and between Oct4A and Sox-transcriptional factors (Sox2, Sox4 or Sox17) in GBM0378 GSCs treated with 2-BP (50 μM) or depalmitoylation inhibitor (PalmB, 2 μM) (right panel) after performing an immunoprecipitation assay. (C) Luciferase reporter assay showed luciferase activities of the reporters driven by the SOX2 enhancer region in the T98G GSCs transfected with Oct4A (wt), Oct4A (C198A), or/and Sox4. (D) Histograms of the relative Oct4A, Sox2, and GFAP mRNA levels in T98G GSCs transfected with Oct4A or enhanced Oct4A plasmids were obtained via real-time reverse transcriptase-polymerase chain reaction. (E) Associations between Oct4A and ZDHHC17 mRNA protein levels in glioblastoma (GBM) (n = 168; TCGA), using cBioPortal. (F) Associations between Oct4A and ZDHHC17 protein levels in GBM tissues (n = 168). (G) Associations between Sox2 and ZDHHC17 protein levels in GBM tissues (n = 168). (H) Immunofluorescent analysis demonstrating colocalization between Oct4A and Lamp1 (a marker for lysosome) in T98G GSCs during the self-renewal or differentiation stage. Scale bars = 25 μm. (I) Immunofluorescent analysis demonstrating colocalization between Oct4A C198A and Lamp1 (a marker for lysosome) in T98G GSCs during the self-renewal stage. Scale bars = 25 μm. (J) Detecting Oct4A protein expression and phosphorylation of Oct4A T343 in T98G GSCs during the self-renewal or differentiation stage by western blotting, and Oct4A palmitoylation level in T98G GSCs in the presence of 50 μM leupeptin by ABE method.

self-renewal of glioma cells due to the upregulation of Sox2-positive cells (Supplementary Figure 5E). When ZDHHC17 expression was knocked down, Sox2 expression was also decreased along with the decrease of Oct4A palmitoylation (Supplementary Figure 5F). These results demonstrate that palmitoylation mediated by ZDHHC17 is essential both for the interaction between Oct4A and Sox4, and to induce Sox2 expression in GSCs.

To probe the effects of depalmitoylation on the trafficking of Oct4A during self-renewal and differentiation of GSCs, we blocked the palmitoylation of Oct4A and studied its distribution in lysosomes. Along with the expression, and its palmitoylation of Oct4A reduction, its colocalization with lysosome-associated membrane protein 1 (Lamp1)-labeled lysosomes increased during the GSCs' differentiation stage (Figure 4H). Similarly, disruption of palmitoylation via the C198A mutation increased the colocalization of Oct4A in the lysosomes, even at the self-renewal stage (Figure 4I). Notably, the stability and phosphorylation of Oct4A might be regulated by its palmitoylation (Figure 4J and Supplementary Figure 5G). These results consistently indicate that depalmitoylation promotes Oct4A degradation through the lysosomal pathway.

Targeting Oct4A Palmitoylation With a Peptidic Inhibitor

After determining the palmitoylation motif of Oct4A, we tried to introduce the competitive inhibitor of palmitoylation of Oct4A into tumor cells. A cell-penetrating peptide containing an Oct4A1 (191-205) palmitoylation sequence (CPP-S1), and a control peptide with the C198A mutation (CPP-S0), were synthesized in vitro. The coimmunoprecipitation assay confirmed that CPP-S1, not CPP-S0, had weakened the interaction between Oct4A and its palmitoyltransferase (ZDHHC17) in a dose-dependent manner (Figure 5A). Additionally, the ABE assay demonstrated that CPP-S1 specifically decreased the palmitoylation of Oct4A (Figure 5B, Supplementary Figure 6). Importantly, the expression of Oct4A decreased at the GSC differentiation stage in a dose-dependent manner. In contrast, no change in Oct4A expression was found in differentiated GSCs incubated with the control CPP-S0 peptide (Figure 5C). These results indicate that CPP-S1 is an Oct4A-targeting molecule, which can competitively inhibit palmitoylation of Oct4A.

To investigate the role of Oct4A palmitoylation on the tumor-initiating potential of GSCs, we attempted to evaluate the rate of tumor formation. First, we subcutaneously injected T98G GSCs into immunocompromised mice via an in vivo serial dilution assay (Table 1), and found that injection of 100 wild-type T98G GSCs could induce the tumor-like phenotype, and the rate of tumor formation was 40%. When more than 300 cells were injected, the tumor formation rate could be greater than 80%. However, Oct4A knockdown (Oct4A shRNA-GSCs) or Oct4A-palmitoylation inhibition (Oct4A C198A-GSCs) could reduce the tumor formation rate, and a tumor could only form if 300 or more cells were injected. And a cell count of 1000 was needed to efficiently induce tumor formation. As expected, treatment with CPP-S1 (25 μg) before injection significantly suppressed tumor formation as compared to that seen in control animals. Consistently, a high dose (50 μg) of CPP-S1 was found to suppress Oct4A-dependent tumor formation efficiently.

At the same time, in order to ensure the tumor formation rate, we selected the experimental protocol of implanting 1000 cells to evaluate the effect of Oct4A palmitoylation on tumor growth and stem cell marker expression. We found that injection of 1000 control T98G cells did not induce the tumor-like phenotype. However, the injection of 1000 GSCs derived from T98G cells resulted in substantial tumor growth, indicating that GSCs have tumor-initiating potential (Figure 5D). Notably, Oct4A knockdown (Oct4A shRNA-GSCs) or Oct4A-palmitoylation inhibition (Oct4A C198A-GSCs) could lead to a decrease in tumor growth (Figure 5E) and weight (Supplementary Figure 7A). Besides, treatment with CPP-S1 (25 μg) before injection significantly suppressed tumor growth (Figure 5D and E) and weight (Supplementary Figure 7A) compared to the control animals. Moreover, a high dose (50 μg) of CPP-S1 was found to suppress Oct4A-dependent tumor growth efficiently. Consistent with this, CCP-S1 effectively suppressed tumor growth (Supplementary Figure 7B) and GFAP- or Sox2-positive cells (Supplementary Figure 7C) in an orthotopic GBM model. At the same time, we used patient-derived GSCs (GBM1492 and GBM0378) to construct a tumor-bearing model and found that successive injections of CPP-S1 to tumor-bearing mice could substantially enhance impact, including inhibition of tumor growth (Supplementary Figure 7D–F) and decrease of Oct4A palmitylation and Sox2 expression (Supplementary Figure 7G).

Next, we performed an intracranial injection of GSCs into immunocompromised mice to determine the effect of Oct4A palmitoylation on GSC tumor-initiating potential. We found that injection of 1000 GBM0378 GSCs resulted in animal death within 10-25 days, and injection of 1000 GBM1492 GSCs resulted in animal death within 20-35 days (Figure 5F). However, injection of 1000 GBM0378 or GBM1492 glioblastoma cells did not result in death of the tumor-bearing mice during the observation period (Figure 5F). As expected, treatment with CPP-S1 before injection extended the survival rate (Figure 5F). As the Oct4A palmitoylation level decreased, Oct4A and Sox2 levels decreased (Figure 5G) and the CD133-positive cell numbers reduced (Figure 5H) in the xenograft model. This was due to the fact that GSCs were pre-treated with CPP-S1. Taken together, these results suggest that treatment with short-term in vitro CPP-S1 was sufficient to reduce the number of tumor-initiating cells in the GSC samples, resulting in delayed tumor development.

Palm-acylated modification promotes the stability of the Oct4A protein, as well as its interaction with Sox4 on the SOX2 enhancer region, to maintain self-renewal and tumorigenicity of GSCs. However, although it can be combined with SOX2, Oct4A is not modified by the palmoylotransferase ZDHHC17 and would be degraded in the lysosomes (Figure 5I).

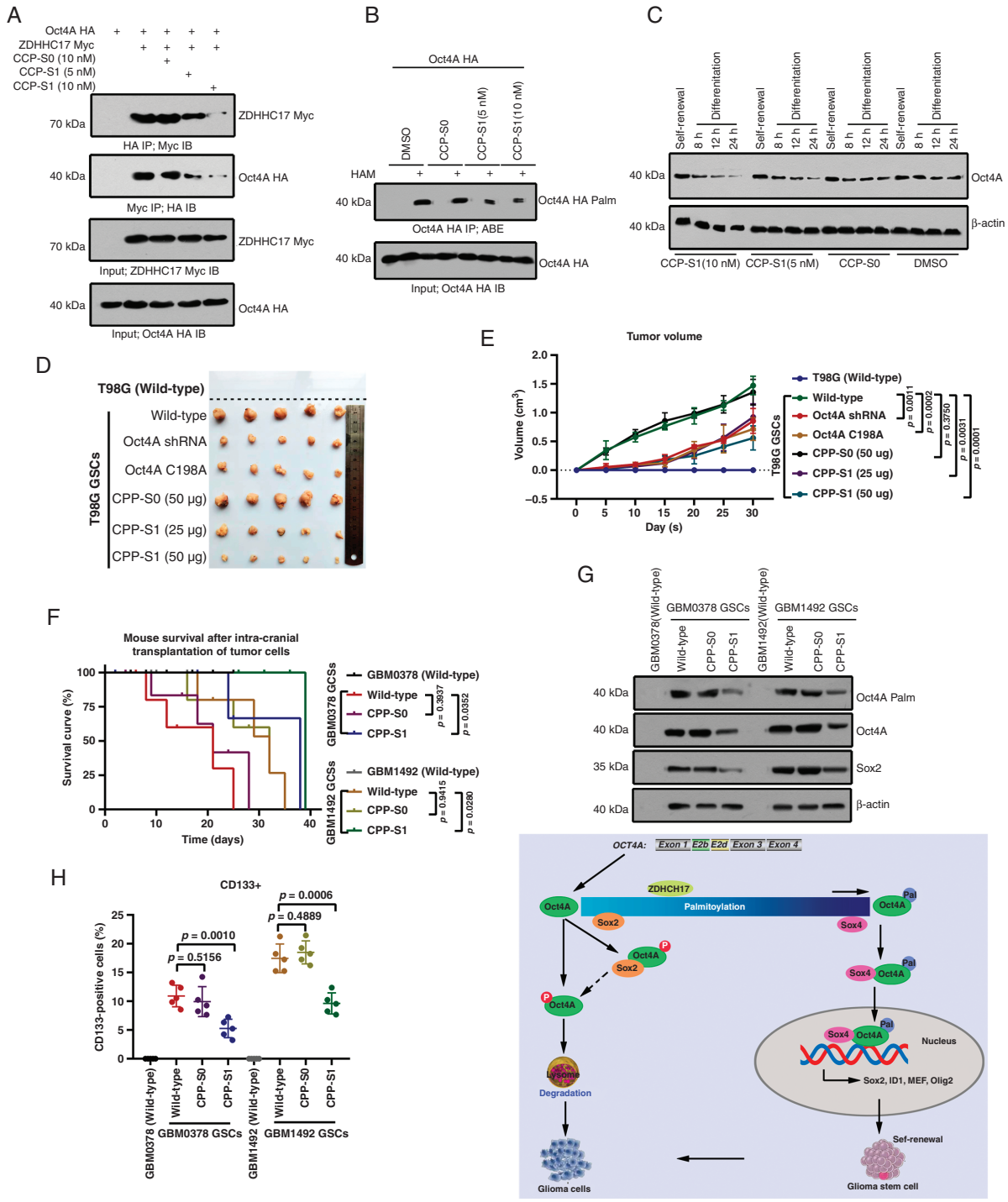

Fig. 5 Targeting Oct4A palmitoylation with a peptidic inhibitor. (A) Detecting the interaction between HA-tagged Oct4A and Myc-tagged ZDHHC17 in HEK293 cells treated with different concentrations of CPP-S1 after performing immunoprecipitation assays. (B) Detection of HA-tagged Oct4A palmitoylation level in HEK293 cells in the presence of different concentrations of CPP-S1 by the ABE method. (C) Detection of Oct4A protein expression in T98G GSCs treated with different concentrations of CPP-S1 during the self-renewal or differentiation stage by western blotting. (D, E) Tumor growth of T98G (inoculation with 1000 cells) and T98G GSCs (inoculation with 1000 cells) transfected with the control and Oct4A shRNA duplex or Oct4A (C198A) and pre-treated with CPP-S0 (50 μg, 72 hours) or different concentrations of CPP-S1 (25 μg and 50 μg; 72 hours) in BALB/c immunocompromised nude mice. Tumor volumes were evaluated at the indicated time points (n = 5 mice/group). (F) Kaplan-Meier survival curve showing the survival of the animals injected with GSCs after CPP-S1 treatment. GBM0378 or GBM1492 GSCs were derived from GBM0378 or GBM1492 patient-derived glioblastoma cells, respectively. GBM0378 glioblastoma cells (inoculation with 1000 cells), GBM0378 GSCs (inoculation with 1000 cells), GBM1492 glioblastoma cells (inoculation with 1000 cells), or GBM1492 GSCs (inoculation with 1000 cells) pre-treated with or without CPP-S0 (50 μg, 72 hours) or different concentrations of CPP-S1 (50 μg, 72 hours) were implanted in BALB/c mouse brains. No death

Discussion

In this study, we reported that all three variants of Oct4 were expressed in different types of brain cancer, and we proved the key role of palmitoyl in regulating the stability of the Oct4A protein; this is important for the maintenance of tumorigenic activity in GSCs. The effects of targeting Oct4A palmitoylation on Oct4A expression, integration between Oct4A and the Sox axis, and tumorigenicity of GSCs, revealed that modulation of this posttranslational modification is a promising therapeutic strategy against cancer stem cells (CSCs).

Cancer is likely to relapse and metastasize if CSCs are not completely eliminated. Previously, CSCs were thought to express markers, such as Wnt, Hedgehog, Notch, phosphatidylinositol 3 kinase (PI3K), mammalian target of rapamycin (mTOR), transforming growth factor-beta (TGF-β), and leukemia inhibitory factor (LIF).[24–27] However, it is now evident that most of these proteins are also expressed by normal stem cells, and targeting them in CSCs would lead to damage to normal stem cells as well, inducing side effects.[28,29] From a clinical point of view, it is therefore important to identify not only factors needed to maintain cancer-initiating cells, but also those that can differentiate cancer cells from normal stem cells.

Here, we identified a regulatory mechanism unique to CSCs. Targeting this regulatory mechanism allows the precise attack of CSCs. This approach is potentially valuable in the development of cancer therapeutic drugs with few or no side effects. Briefly, palmitoylation of Oct4A induces formation of the Oct4A-Sox4 complex and activates the enhancer region of the *SOX2* gene, a key gene for maintaining the tumorigenicity of GSC, to maintain the stemness of CSCs in a positive regulatory loop. Both Oct4A and Sox2 are important in maintaining normal stem cell or CSC self-renewal.[30,31] In CSCs, Sox2 does not mainly exist in the transcription factor complex of the *SOX2* enhancer region. Instead, Sox4 forms a transcription complex with Oct4A that activates the enhancer region of *SOX2*. These findings suggest that upregulation of Sox4 enhances the expression of Sox2 in GSC, which is regulated by a self-reinforcing regulatory loop in neural progenitor cells and is relatively independent. In fact, the integration of the Sox axis and Oct4A is mainly regulated by the palmitoyl state of Oct4A. Palmitoylated Oct4A interacts with Sox4 to potentiate *SOX2* enhancer activity, whereas palmitoyl-mutant Oct4A mainly interacts with Sox2.

Palmitoylation in proteins is dynamically regulated by palmitoyltransferase and acyl-protein thioesterase.[32,33] Recent studies reveal that the ZDHHC family, including ZDHHC5/17/18/23, exhibits different functions when regulating the malignant development and progression of glioma[15,16,34]; we observed that palmitoyltransferase ZDHHC17 regulated the palmitoylation and stability of Oct4A. Previous studies found that ZDHHC17 interacts with MAP2K4 through N-terminal signal transduction and protein-protein interaction, and plays an obvious and unique role in the palmitoyl acyltransferase (PAT) protein family to activate c-Jun N-terminal kinase (JNK)/p38 and regulate the development and progress of malignant GBM.[33] GSC self-renewal mediated by ZDHHC17 showed a preference for JNK activation because neither a p38 agonist nor a phosphor-p38 inhibitor was able to offset the interruption of GSC maintenance or inhibit GSC self-renewal induced by ZDHHC17 depletion, respectively.

Although PAT—a transmembrane S-acyltransferase—contains a conserved zinc finger (DHHC) domain, few PAT inhibitors (especially DHHC isomer-specific inhibitors) are available.[35,36] As mature lipid-based 2-BP is a nonspecific inhibitor, it can block the palmitoyltransferase activity of all evaluated DHHC proteins and increase the risk of unknown side effects.[37,38] Although competitive inhibition is effective in targeting specific enzymes, it seems this strategy has not been widely used to inhibit DHHC acetyltransferase.[39,40] After determining the palmitoylation motif of Oct4A, we tried to design a short substrate sequence to competitively inhibit the palmitoylation of endogenous Oct4A. The Oct4A1 (191-205) sequence containing the palmitoyl motif (CPP-S1), rather than the control sequence containing the C198A mutation (CPP-S0), exhibits membrane binding; this is a characteristic of palmitoyl proteins. In addition, the ABE assay indicated that CPP-S1 was palmitoylated, but CPP-S0 was not. Therefore, CPP-S1 reduced palmitoylation of Oct4A. In addition, CPP-S1 can inhibit tumor growth from Oct4A-mediated GSCs. Furthermore, we tested the toxicity of competitive peptides in mice. In fact, compared with the mice in the control group, all five mice injected with CPP-S1 (25 μg or higher) survived to the endpoint (4 weeks after injection). We did not find any difference in the overall appearance of live mice between groups. This attempt may provide a unique way to develop Oct4A inhibitors.

In conclusion, Oct4A is the key factor in maintaining the tumorigenic activity of GSCs. Palmitoylation mediated by ZDHHC17 was indispensable for keeping Oct4A from lysosomal degradation to maintain its protein stability and was beneficial to the formation of complexes between Sox4 and Oct4A. These findings identify palmitoylation as a key means to regulate the stability of Oct4A. Palmitoylation of Oct4A mediated by ZDHHC17 acetyltransferase was identified as a promising therapeutic approach toward effectively eliminating cancer-initiating cells. Moreover, they fully reveal the molecular mechanisms of protein stability and the self-renewal function of Oct4A in the progression of gliomas. Our findings suggest a potential strategy to target CSCs with precision, which could be used to develop cancer drugs with fewer side effects.

Fig. 5 Continued

occurred in nude mice after intracranial inoculation of 1000 GBM0378 or GBM1492 glioblastoma cells. CPP-S1 pre-treatment efficiently extended the survival of all animals injected with the corresponding GSCs. (G) Detection of Oct4A and Sox2 expression levels and Oct4A palmitoylation level in intracranial tumors (F) using western blotting and ABE method, respectively. (H) Detection and quantitation of CD133 (stem cell marker)-positive cells in intracranial tumors (F) via flow cytometry. (I) Schematic representation demonstrating that Oct4A is a factor of crucial importance for the maintenance of tumorigenic activity in glioma stem cells. Palmitoylation mediated by ZDHHC17 was deemed indispensable for keeping Oct4A from lysosomal degradation to maintain its protein stability and was beneficial for complexes between Sox4 and Oct4A.

Table 1. Role of Oct4A Palmitoylation on the Tumor-initiating Potential of GSCs

Oct4A	Number of Implanted Cells	Rate of Tumor Formation (Day 20, >0.2 cm^3)
Wild-type	**100**	**2/5** (40%)
	200	**3/5** (60%)
	300	**4/5** (80%)
	500	**5/5** (100%)
	1000	**5/5** (100%)
	5000	**5/5** (100%)
Oct4A shRNA	100	0/5 (0%)
	200	0/5 (0%)
	300	**2/5** (40%)
	500	**2/5** (40%)
	1000	**5/5** (100%)
	5000	**5/5** (100%)
Oct4A C198A	100	0/5 (0%)
	200	0/5 (0%)
	300	**1/5** (20%)
	500	**2/5** (40%)
	1000	**5/5** (100%)
	5000	**5/5** (100%)
CPP-S0 (50 μg)	**100**	**1/5** (20%)
	200	**3/5** (60%)
	300	**4/5** (80%)
	500	**4/5** (80%)
	1000	**5/5** (100%)
	5000	**5/5** (100%)
CPP-S1 (25 μg)	100	0/5 (0%)
	200	0/5 (0%)
	300	**2/5** (40%)
	500	**3/5** (60%)
	1000	**5/5** (100%)
	5000	**5/5** (100%)
CPP-S1 (50 μg)	100	0/5 (0%)
	200	0/5 (0%)
	300	**1/5** (20%)
	500	**2/5** (40%)
	1000	**4/5** (80%)
	5000	**5/5** (100%)

Day 20, 20 days after subcutaneous transplantation; >0.2 cm^3, the tumor volume was greater than 0.2 cm3.
Values in bold style was labeled tumor formation.

Supplementary Material

Supplementary material is available at *Neuro-Oncology* online.

Keywords

glioma stem cells (GSCs) | glioblastoma multiforme | Oct4A | palmitoylation | Sox2

Funding

This research was supported by the National Natural Science Foundation of China (grant numbers 82172663, 82104208, 81872066, 81773131, and 81972635), the Youth Innovation Promotion Association of the Chinese Academy of Sciences (grant number 2018487), the Innovative Program of Development Foundation of Hefei Centre for Physical Science and Technology (grant number 2021HSC-CIP011), and the National Key R&D Program of China (grant number 2017YFA0503600).

Acknowledgments

We thank the members of the technical assistance team at the Institute of Health and Medical Technology, Hefei Institutes of Physical Science, Chinese Academy of Sciences. We also thank Dr. Fukata for providing the 23 plasmids encoding the HA-tagged ZDHHC family proteins.

Conflict of interest statement. None of the authors have any potential conflicts of interest to disclose.

Authorship statement. Z.F. and X.C. conceived and designed the experiments; X.C., X.F., W.N., H.Y., C.Z., and J.F. performed the experiments; X.F., H.Y., and X.C. analyzed the data; X.C., X.F., and W.N. wrote the paper. X.C., W.N., X.Y., and Z.F. revised the manuscript. All authors read and approved the final manuscript.

Ethics Approval and Consent to Participate

The study was approved by the Institutional Review Board of Hefei Cancer Hospital, Chinese Academy of Sciences (approval number, SWYX-Y-2021-41). All animal experiments were performed according to the guidelines of the Animal Use and Care Committees at the Hefei Institutes of Physical Science, Chinese Academy of Sciences (approval number, SWYX-DW-2021-37).

Consent for Publication

Not applicable.

Data Availability

All data generated or analyzed during this study are included in this article.

References

1. McFaline-Figueroa JR, Lee EQ. Brain tumors. *Am J Med.* 2018;131(8):874–882.
2. Yang K, Wu Z, Zhang H, et al. Glioma targeted therapy: insight into future of molecular approaches. *Mol Cancer.* 2022;21(1):39.
3. Osuka S, Van Meir EG. Overcoming therapeutic resistance in glioblastoma: the way forward. *J Clin Invest.* 2017;127(2):415–426.
4. Prager BC, Bhargava S, Mahadev V, Hubert CG, Rich JN. Glioblastoma stem cells: driving resilience through chaos. *Trends Cancer.* 2020;6(3):223–235.
5. Pan GJ, Chang ZY, Schöler HR, Pei D. Stem cell pluripotency and transcription factor Oct4. *Cell Res.* 2002;12(5–6):321–329.
6. Niwa H, Miyazaki J, Smith AG. Quantitative expression of Oct-3/4 defines differentiation, dedifferentiation or self-renewal of ES cells. *Nat Genet.* 2000;24(4):372–376.
7. Wang X, Dai J. Concise review: isoforms of OCT4 contribute to the confusing diversity in stem cell biology. *Stem Cells.* 2010;28(5):885–893.
8. Radzisheuskaya A, Silva JC. Do all roads lead to Oct4? The emerging concepts of induced pluripotency. *Trends Cell Biol.* 2014;24(5):275–284.
9. Villodre ES, Kipper FC, Pereira MB, Lenz G. Roles of OCT4 in tumorigenesis, cancer therapy resistance and prognosis. *Cancer Treat Rev.* 2016;51(1):1–9.
10. Liu T, Xu H, Huang M, et al. Circulating glioma cells exhibit stem cell-like properties. *Cancer Res.* 2018;78(23):6632–6642.
11. Daniotti JL, Pedro MP, Valdez Taubas J. The role of S-acylation in protein trafficking. *Traffic.* 2017;18(11):699–710.
12. Korycka J, Lach A, Heger E, et al. Human DHHC proteins: a spotlight on the hidden player of palmitoylation. *Eur J Cell Biol.* 2012;91(2):107–117.
13. Resh MD. Palmitoylation of proteins in cancer. *Biochem Soc Trans.* 2017;45(2):409–416.
14. Ko PJ, Dixon SJ. Protein palmitoylation and cancer. *EMBO Rep.* 2018;19(10):e46666.
15. Chen X, Ma H, Wang Z, et al. EZH2 palmitoylation mediated by ZDHHC5 in p53-mutant glioma drives malignant development and progression. *Cancer Res.* 2017;77(18):4998–5010.
16. Chen X, Hu L, Yang H, et al. DHHC protein family targets different subsets of glioma stem cells in specific niches. *J Exp Clin Cancer Res.* 2019;38(1):25.
17. Perzel Mandell KA, Eagles NJ, Wilton R, et al. Genome-wide sequencing-based identification of methylation quantitative trait loci and their role in schizophrenia risk. *Nat Commun.* 2021;12(1):5251.
18. Ferrari F, Arrigoni L, Franz H, et al. DOT1L-mediated murine neuronal differentiation associates with H3K79me2 accumulation and preserves SOX2-enhancer accessibility. *Nat Commun.* 2020;11(1):5200.
19. Schmidt MF, Gan ZY, Komander D, Dewson G. Ubiquitin signalling in neurodegeneration: mechanisms and therapeutic opportunities. *Cell Death Differ.* 2021;28(2):570–590.
20. Rafiq S, McKenna SL, Muller S, Tschan MP, Humbert M. Lysosomes in acute myeloid leukemia: potential therapeutic targets? *Leukemia.* 2021;35(10):2759–2770.
21. Zhu Z, Mesci P, Bernatchez JA, et al. Zika virus targets glioblastoma stem cells through a SOX2-integrin α(v)β(5) axis. *Cell Stem Cell.* 2020;26(2):187–204.e10.
22. Bageritz J, Puccio L, Piro RM, et al. Stem cell characteristics in glioblastoma are maintained by the ecto-nucleotidase E-NPP1. *Cell Death Differ.* 2014;21(6):929–940.
23. Zhang LH, Yin YH, Chen HZ, et al. TRIM24 promotes stemness and invasiveness of glioblastoma cells via activating Sox2 expression. *Neuro Oncol.* 2020;22(12):1797–1808.
24. Ratajczak MZ, Bujko K, Mack A, Kucia M, Ratajczak J. Cancer from the perspective of stem cells and misappropriated tissue regeneration mechanisms. *Leukemia.* 2018;32(12):2519–2526.
25. Lucena-Cacace A, Otero-Albiol D, Jiménez-García MP, Muñoz-Galvan S, Carnero A. *NAMPT* is a potent oncogene in colon cancer progression that modulates cancer stem cell properties and resistance to therapy through Sirt1 and PARP. *Clin Cancer Res.* 2018;24(5):1202–1215.
26. Haynes J, McKee TD, Haller A, et al. Administration of hypoxia-activated prodrug evofosfamide after conventional adjuvant therapy enhances therapeutic outcome and targets cancer-initiating cells in preclinical models of colorectal cancer. *Clin Cancer Res.* 2018;24(9):2116–2127.
27. Du L, Cheng Q, Zheng H, et al. Targeting stemness of cancer stem cells to fight colorectal cancers. *Semin Cancer Biol.* 2021;82(1):150–161.
28. Paul R, Dorsey JF, Fan Y. Cell plasticity, senescence, and quiescence in cancer stem cells: biological and therapeutic implications. *Pharmacol Ther.* 2021;231(1):107985.
29. Sharifzad F, Ghavami S, Verdi J, et al. Glioblastoma cancer stem cell biology: potential theranostic targets. *Drug Resist Updat.* 2019;42(1):35–45.
30. Velychko S, Adachi K, Kim KP, et al. Excluding Oct4 from Yamanaka cocktail unleashes the developmental potential of iPSCs. *Cell Stem Cell.* 2019;25(6):737–753.e4.
31. Bertolini JA, Favaro R, Zhu Y, et al. Mapping the global chromatin connectivity network for Sox2 function in neural stem cell maintenance. *Cell Stem Cell.* 2019;24(3):462–476.e6.
32. Tsutsumi R, Fukata Y, Fukata M. Discovery of protein-palmitoylating enzymes. *Pflugers Arch.* 2008;456(6):1199–1206.
33. Nadolski MJ, Linder ME. Protein lipidation. *FEBS J.* 2007;274(20):5202–5210.
34. Chen X, Hao A, Li X, et al. Activation of JNK and p38 MAPK mediated by ZDHHC17 drives glioblastoma multiforme development and malignant progression. *Theranostics.* 2020;10(3):998–1015.
35. Lanyon-Hogg T, Faronato M, Serwa RA, Tate EW. Dynamic protein acylation: new substrates, mechanisms, and drug targets. *Trends Biochem Sci.* 2017;42(7):566–581.
36. De I, Sadhukhan S. Emerging roles of DHHC-mediated protein S-palmitoylation in physiological and pathophysiological context. *Eur J Cell Biol.* 2018;97(5):319–338.
37. Lan T, Delalande C, Dickinson BC. Inhibitors of DHHC family proteins. *Curr Opin Chem Biol.* 2021;65(1):118–125.
38. Azizi SA, Kathayat RS, Dickinson BC. Activity-based sensing of S-depalmitoylases: chemical technologies and biological discovery. *Acc Chem Res.* 2019;52(11):3029–3038.
39. Yao H, Lan J, Li C, et al. Inhibiting PD-L1 palmitoylation enhances T-cell immune responses against tumours. *Nat Biomed Eng.* 2019;3(4):306–317.
40. Davda D, El Azzouny MA, Tom CT, et al. Profiling targets of the irreversible palmitoylation inhibitor 2-bromopalmitate. *ACS Chem Biol.* 2013;8(9):1912–1917.